RSC Advances

PAPER

View Article Online
View Journal | View Issue



Cite this: *RSC Adv.*, 2023, **13**, 22481

# Optical properties of nanostructured antiviral and anticancer drugs†

Alessandra Angela Pisu,‡[a] Francesco Siddi,‡[a] Giancarlo Cappellini *[ab] and Roberto Cardia *[a]

We present a computational study on the optical absorption properties of some systems of interest in the field of drug delivery. In particular we considered as drug molecules favipiravir (T705, an antiviral molecule) and 5-fluorouracil (5FU, an anticancer molecule) and, on the other hand, pure fullerenes ($C_{24}$, $B_{12}N_{12}$, $Ga_{12}N_{12}$) and doped fullerenes ($C_{23}B$, $CB_{11}N_{12}$) are considered as nanocarriers. Some combined configurations between the drug molecules and the carrier nanostructures have been then studied. The optical absorption properties of the above mentioned drug molecules and their carrier nanostructures in the free and bound states are obtained by a TD-DFT method, in gas phase and in aqueous solution. We perform a detailed analysis of the modifications arising in the absorption spectra that take place in some linked configurations between the drug molecules and the carrier nanostructures. These changes could be of importance as an optical fingerprint of the realized drug/carrier link.

Received 4th January 2023
Accepted 30th June 2023

DOI: 10.1039/d3ra00061c

rsc.li/rsc-advances



## 1. Introduction

In recent years, the nanostructures based on carbon, boron nitride, gallium nitride and derivatives have been subject of great interest in the scientific community. These systems can be promising candidates to face several issues and emerging challenges in technological fields, ranging from the biological to medical and electronics ones.[1–8] In this work we focus our attention on small fullerenes based on C, BN e GaN, here considered as potential carriers of the drugs T705 and 5FU.

Favipiravir (T705 for short, $C_5H_4FN_3O_2$) is a molecule of strong pharmacological interest, developed in Japan in 1999, that is used in different kinds of biological areas for its antiviral proprieties. Favipiravir acts as broad-spectrum inhibitor against many different RNA viruses. Its action is based on the inhibition of the RNA polymerase and as a consequence it blocks the replication of the virus.[9–11] Its first significant application was in the cure of Ebola outbreak,[12] and today its effects are studied as possible cure against SARS-CoV-2 virus.[13]

5-Fluorouracil (shortly 5FU and chemical formula $C_4H_3FN_2O_2$) is a fluorinate analogue of pyrimidine.[6] It has uracil-like structure, with a peripheral fluorine atom in place of a hydrogen atom. This biomolecule is often used in chemotherapeutic drugs to attack certain types of cancer (*e.g.*, skin, breast, stomach, colon cancers).[6,14–18] Its mechanism of action is based on entering and interfering in the synthesis process of nucleic acids (DNA, RNA) of the tumoral cells. Therefore, the replication of tumoral cells is inhibited.

The carbon based fullerenes ($C_{2n}$) can be formed by $2n$ C atoms linked together with covalent bonds.[4] The most famous and representative carbon fullerene is $C_{60}$, discovered in 1985 by Kroto[19] (Nobel Prize in Chemistry, 1996).[20] After the discovery of $C_{60}$, researchers have shown increasing interest in finding new fullerenes. During the years, several studies on the stability of fullerenes with $2n < 60$ and $2n > 60$ have been done. Many of these systems have been also synthesized[21–23] within several techniques like arc-melting, laser ablation and electron beam irradiation technique.[4,24–29] In recent years, small fullerenes (such as the $C_{24}$ considered in this work) have gained the attention of the researchers. The fullerene $C_{24}$ has been studied in several works to prove its stability and to understand its properties.[21,30] In 2002, $C_{24}$ has been synthesized within the electron beam irradiation technique.[31,32] Boron nitride fullerenes can be formed by the same number of B and N atoms ($B_nN_n$), linked together with polar B–N bonds. Boron nitride fullerenes are isoelectronic with respect the carbon fullerenes formed of the same number of atoms. Their interesting chemical, physical, optical, electronics properties are different from the ones of their C counterparts. Boron nitride fullerenes are widely studied in several theoretical works[30,33,34] and most of them have been also synthesized.[31,35–37] The most stable system of the $B_nN_n$ family is $B_{12}N_{12}$,[33,34] which has been synthesized in 1998 within the electron beam irradiation.[36,37]

Gallium nitride nanocages ($Ga_xN_x$, with $10 \leq x \leq 20$) have been analyzed theoretically in ref. 7, to demonstrate their

[a]*Department of Physics, University of Cagliari, S.P. Monserrato-Sestu Km 0,700, Monserrato, CA I-09042, Italy. E-mail: giancarlo.cappellini@dsf.unica.it; roberto.cardia@dsf.unica.it*

[b]*European Theoretical Spectroscopy Facility (ETSF), Italy*

† Electronic supplementary information (ESI) available. See DOI: https://doi.org/10.1039/d3ra00061c

‡ These authors contributed equally to this work.

stability and physical properties. In this work we consider the GaN fullerene of 24 atoms, $Ga_{12}N_{12}$.

The unique chemical and physical properties of C and BN fullerenes are manifold: good adsorption capacity and interaction with bio/pharmaceutical molecules, high chemical stability, easiness of functionalization, biocompatibility, low toxicity and low poisonous quality.[1,2,9,38,39] These properties make the C/BN fullerenes interesting for potential applications in biomedical fields as sensors (drug detectors) and transporter of drugs (drug carriers).[1,2,9,39] Moreover, the good adsorption propriety allows the fullerenes to capture small molecules and to interact with them with high energy bond. Therefore, several researchers investigated the possibility to use them as gas sensors for the detection of harmful and polluting substances.[2,33,38–41] Furthermore, GaN nanostructures are promising candidate for new nanotechnology applications.[7] Gallium nitride systems are used in some optoelectronic devices and applications. For example, they can be used in light-emitting devices.[7,8]

An emerging challenge in the biomedical field is the research of systems based on nanostructures for the drug delivery. This is a promising modality to face and to overcome some problems related to the traditional way of drug administration.[1,42] This innovative way of delivery consists in using nanostructures, such as functionalized fullerenes, as support system for bio/pharmaceutical molecules: the loaded drug will be transported by the carrier toward a specific target and will be released in the desired zone. As a consequence, the side effects are reduced and the quality of the therapy improves. The release mechanism can happen in several ways, for example through the action of enzymes or for particular pH conditions.[1,6,42,43] In antiviral and antitumoral therapy there are needs of research and development in the drug delivery field. In particular, the efficiency of some clinical antiviral drugs is limited because of several factors: drug resistance, poor bioavailability, weak solubility and permeability, release off target, harmful side effects.[9,44,45] Concerning the antitumoral therapy, the chemotherapy performed with traditional mechanism can be very harmful for the patient. The limitations are related to: drug toxicity and low solubility, degradation of drug before reaching the target, tumoral cell drug resistance, lack of selectivity between healthy and sick cells and release off target.[46–48] In antiviral and antitumoral therapy a suitable drug delivery based on nanostructures (fullerenes, nanotubes, graphene-like structures), can improve the selectivity, facilitate the penetration of polar drugs through the cells, increase the drug release at the target.[9,43–45] Moreover, they permit lower dosage and, therefore, less side effects[6,9] and less damage to the healthy cells.[6,46]

Regarding the drug delivery based on fullerenes, the best known involves the $C_{60}$, and in scientific literature there are several works concerning *in vitro* and *in vivo* tests.[1,49,50] In particular, in these experiments, functionalized $C_{60}$ is considered as a carrier of biomolecules that can be either adsorbed on the external surface of the carrier[1,50] or loaded inside the $C_{60}$.[49] For smaller fullerenes like $C_{24}$ and $B_{12}N_{12}$, several DFT and TD-DFT studies are being conducted to evaluate their potential applicability in this field.[9,33,38,43,51] Concerning the gallium nitride $Ga_{12}N_{12}$ nanocage, in recent years its potential action as carrier for anticancer drugs 5-fluorouracil[6] and cisplatin[52] has been studied.

The aim of this work is to investigate the optical absorption properties obtained by TD-DFT calculations, of some proposed drug delivery systems (carrier + drug). In particular, we built four combined configurations of C/BN fullerenes ($C_{24}$, $B_{12}N_{12}$, $C_{23}B$, $CB_{11}N_{12}$) covalently bonded to 5FU. We considered as potential carrier also two substituted systems ($C_{23}B$ and $CB_{11}N_{12}$). This procedure is justified by the existence of some works in the literature in which it has been demonstrated that the doping process can enhance the interaction between carrier and drug.[1,9,33,43]

To validate our methods we considered some configurations from the scientific literature (C/BN clusters-T705 and $Ga_{12}N_{12}$-5FU).[6,9] Please consider that it is out of the scope of this work to enter in the complex mechanism of drug delivery made by different steps as the drug/carrier bond creation, the drug transportation and the drug release at the target. Moreover, we do not consider here the issue related to the formation of drug/carrier systems starting from the free components. We focus here on the differences arising in the absorption spectra of the drug/carrier systems considered in their ground-state (either here calculated or obtained from literature) in comparison with the spectra of the free drug and carrier. These differences can be interpreted as an optical fingerprint of the occurred molecular bond between the carrier and the drug molecules.

## 2. Computational details

In this work we performed density functional theory (DFT) and time dependent-DFT (TD-DFT)[53–57] calculations within the Gaussian16 computational code,[58] an all-electron Gaussian-based software package. For all calculations we used a localized Gaussian basis-set (6-31+G*)[59] combined with a hybrid exchange correlation (XC) functional (Becke-3-parameter-Lee–Yang–Parr, B3LYP).[60,61] The chosen basis-set is composed by a valence double-$\zeta$ set including *d* polarization functions (indicated with the symbol "*") and diffuse functions ("+") for each atom other than H. The selected couple of XC potential and basis-set has been successfully tested for many different atomic systems, both organic and inorganic, with different sizes and degrees of complexity.[62–77] Moreover, in several works (which studied nanostructures similar to ours)[6,9,41,51,78] the B3LYP XC functional or the 6-31+G* basis-set have been used.

We performed all the calculations for all systems under study both in gaseous phase and in aqueous solution. For the gas phase calculations we used the default self-consistency field (SCF) method. We investigated the solvent effect of water using the self-consistency reaction field (SCRF) method based on the conductor-like polarizable continuum model (CPCM).[79] In this calculation scheme, the solvent is treated as a conductor-like polarizable continuous medium, described by a dielectric constant other than 1, *i.e.* 78.3553 for water.[58]

In more detail, we have performed geometry optimization of all the structures, in free and bound state, both in gaseous phase and aqueous solution. The configurations obtained from

 

the literature were already optimized, so we did not perform the structural optimization in those cases. In particular for the systems studied in ref. 9 we started from their equilibrium geometry obtained in vacuum. For the systems (drug + carrier) considered in ref. 6 we used their equilibrium geometries obtained in water solution. We used the default convergence criteria as implemented in Gaussian16:[58] maximum force 0.000450 Ha bohr$^{-1}$, RMS force 0.000300 Ha bohr$^{-1}$, maximum displacement 0.001800 Å e RMS displacement 0.001200 Å.

As mentioned in the introduction, in this work we studied some systems of interest for drug delivery. In particular the antiviral drug is the favipiravir (T705) and the anticancer drug is the pyrimidine analogue 5-fluorouracil (5FU), shown in Fig. 1a and b. The nanostructures here analyzed are the carbon-based fullerene $C_{24}$, the boron nitride one $B_{12}N_{12}$, the substituted systems $C_{23}B$ and $CB_{11}N_{12}$ and the gallium nitride nanocage $Ga_{12}N_{12}$ (Fig. 1c–g). We considered three sets of combined systems (Fig. 2), two sets obtained from the literature[6,9] and one set original calculated in the present work.

In particular, we analyzed:

• four configurations after ref. 9: the most stable configurations of T705 adsorbed on the surface of the pure and doped carbon/boron–nitride fullerenes (Fig. 2a–d);

• two configurations after ref. 6: one linked system $Ga_{12}N_{12}$-5FU (Fig. 2e) and one covalent bonded system (Fig. 2f);

• four original configurations: these systems have been obtained by the removal of a hydrogen atom of the 5-fluorouracil molecule to create a covalent bond with the pure and doped C/BN clusters (Fig. 2g–j). Take in consideration that the removal of H atoms in the adsorption of molecules at solid surfaces has been demonstrated in different cases.[80–83]

It is worth mentioning that the systems $C_{23}B$-T705, $CB_{11}N_{12}$-T705, $C_{24}$-5FU and $B_{12}N_{12}$-5FU (respectively shown in Fig. 2c, d, g and h), show states with different multiplicity (and free radical character) due to the presence of unpaired electrons.

Through the DFT we obtained also HOMO (highest occupied molecular orbital) and LUMO (lowest unoccupied molecular orbital) energies, their spatial distribution and their energy gap.

Moreover, the time-dependent counterpart (TD-DFT) of this method has allowed us to obtain the adsorption spectra of the systems. All the TD-DFT calculations were performed in the frequency space within the Casida scheme[55] implemented in the Gaussian16 code. In all DFT and TD-DFT calculations we used the default integration grid and the default convergence criteria for SCF cycles ($10^{-6}$ Hartree for energy differences).

It is well known (for example after ref. 84) that the use of (semi)-local XC (even hybrid) functionals in the standard DFT framework provides a sub-optimal description in the case of transitions with charge transfer (CT) character which need more advanced techniques (*e.g.*, generalized KS framework with

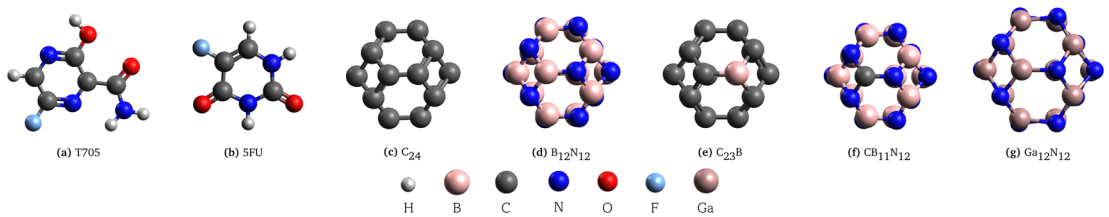


Fig. 1 Optimized geometry of the drug molecules (a) T705, (b) 5FU and of the carrier nanostructures (c) $C_{24}$, (d) $B_{12}N_{12}$, (e) $C_{23}B$, (f) $CB_{11}N_{12}$, (g) $Ga_{12}N_{12}$. Below we have reported the colors table (please consider that Boron and Gallium are of similar color).

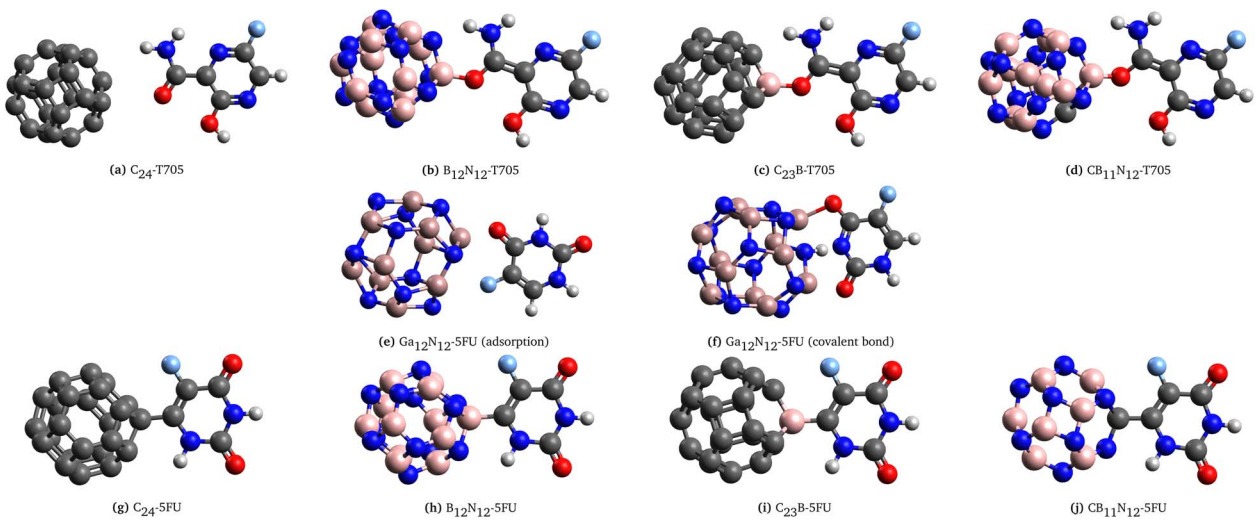


Fig. 2 Optimized geometries of combined systems: (a–d) T705 with pure and doped C/BN carrier after ref. 9 (e and f) 5FU with $Ga_{12}N_{12}$ as carrier after ref. 6, (g–j) 5FU with pure and doped C/BN carrier.

tuned range-separated hybrid XC functionals). We decided to maintain this level of theory because we consider this work as a first approach to the problem and because there is only a small number of excitations with CT character. In the future, we will extend the present study with other calculations, *e.g.*, with more advanced schemes.

## 3. Optical properties

In the present study we considered, for the first two groups of molecules (Fig. 2a–f), six combined clusters which have been demonstrated stable after the computational studies by other groups (ref. 9 and 6). The remaining four combined clusters (Fig. 2g–j) result as stable geometries after the present study. We stress again that the present research is focused on the optical absorption properties of the clusters and not on the search of their particular ground-state configurations. In particular we are interested in the differences in optical absorption properties between free and combined clusters, in case these differences could be considered as optical signature of the realized drug/carrier link.

To this aim, from Fig. 3 to 5 we have reported the absorption spectra of the particular combined systems compared to those of the free molecules (carrier and drug), as obtained after TD-DFT calculations in gas phase. In each plot we showed also the spectra of the combined system in aqueous solution to investigate the solvent effect. In Tables 1 and 2 we analyzed some details of two important peaks of the spectra of the free and bound systems: the first peak (optical onset) and the main peak in the region under study (MP).§ In particular, we have reported: the excitation energy ($E$, eV) and wavelength ($\lambda$, nm) of the transition; the corresponding oscillator strength (O.S.); the occupied and virtual molecular orbitals contributing significantly to the transition (with the corresponding weight in brackets); the character of charge-transfer (CT) or locally-excited (LE) depending on whether or not there is charge transfer upon the transition (Table 2, gas phase column).

For the implicit solvent calculations is important to highlight that in the classical linear response scheme of the polarizable continuum model (PCM) the TD-DFT transition densities are easily available in all conventional TD-DFT calculation schemes and are used to predict the PCM modifications in charges upon excitation. Hence, within this framework the bulk solvent effects for excited states present a moderate computational cost. However, this linear response model is not always accurate in the cases in which are present strong variations of the electronic cloud between the two states involved in a transition; this is the typical case of states with significant charge-transfer as in some of the systems under study in this work (See ESI†). For such cases, more elaborated models to determine the polarization of the cavity in the excited states are used even if is well known that these models are significantly more expensive, from the computational point of view, with respect to

§ Please note that for T705 we reported three peaks instead of two because depending on the spectral region under study the main peak could be at higher energy.

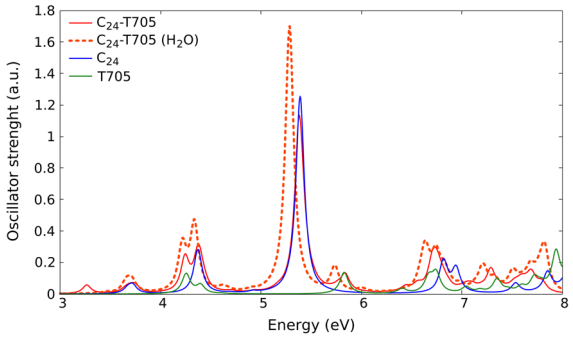


**(a)** Gas-phase absorption spectra of $C_{24}$-T705 (red line), $C_{24}$ (blue line) and T705 (green line). The spectrum of $C_{24}$-T705 in aqueous solution is reported in dotted red line.

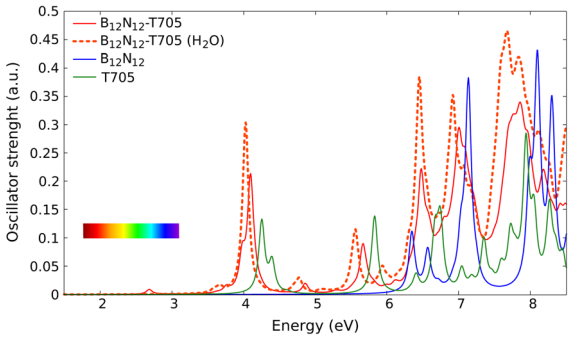


**(b)** Gas-phase absorption spectra of $B_{12}N_{12}$-T705 (red line), $B_{12}N_{12}$ (blue line) and T705 (green line). The spectrum of $B_{12}N_{12}$-T705 in aqueous solution is reported in dotted red line.

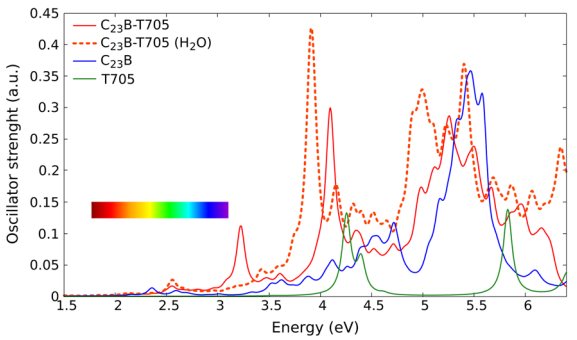


**(c)** Gas-phase absorption spectra of $C_{23}B$-T705 (red line), $C_{23}B$ (blue line) and T705 (green line). The spectrum of $C_{23}B$-T705 in aqueous solution is reported in dotted red line.

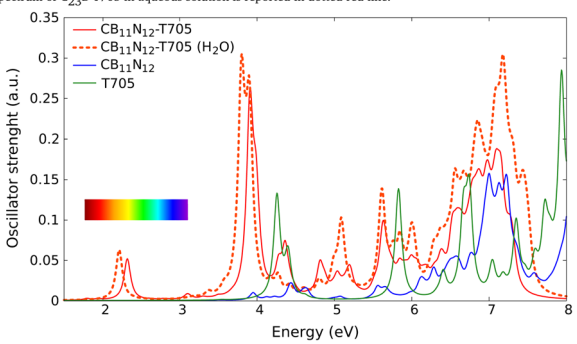


**(d)** Gas-phase absorption spectra of $CB_{11}N_{12}$-T705 (red line), $CB_{11}N_{12}$ (blue line) and T705 (green line). The spectrum of $CB_{11}N_{12}$-T705 in aqueous solution is reported in dotted red line.

Fig. 3 Absorption spectra of the combined systems (a) $C_{24}$-T705, (b) $B_{12}N_{12}$-T705, (c) $C_{23}B$-T705, (d) $CB_{11}N_{12}$-T705 after ref. 9, compared to those of the free molecules (C/BN-carrier and T705). The spectra reported in solid line are calculated in gas phase while in dotted red line is shown the one of combined clusters in aqueous solution. The color bars in the (b–d) figures represent the visible region.

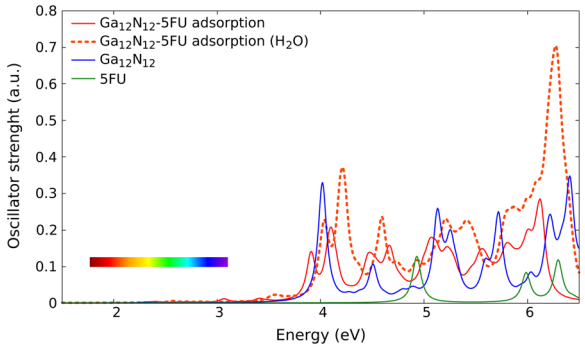


(a) Gas-phase absorption spectra of the adsorption system $Ga_{12}N_{12}$-5FU (red line), $Ga_{12}N_{12}$ (blue line) and T705 (green line). In dotted red line is shown the spectrum of $Ga_{12}N_{12}$-5FU in aqueous solution.

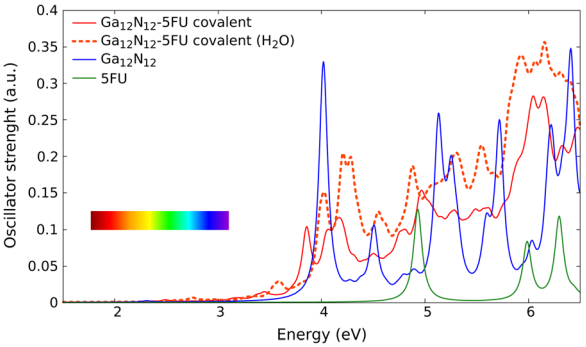


(b) Gas-phase absorption spectra of the covalent system $Ga_{12}N_{12}$-5FU (red line), $Ga_{12}N_{12}$ (blue line) and T705 (green line). In dotted red line is shown the spectrum of $Ga_{12}N_{12}$-5FU in aqueous solution.

Fig. 4 Absorption spectra of the combined systems $Ga_{12}N_{12}$-5FU (a) with adsorption interaction and (b) with covalent bond after ref. 6, compared to those of the free molecules ($Ga_{12}N_{12}$ carrier and 5FU). The spectra reported in solid line are calculated in gas phase while in dotted red line is shown the one of combined clusters in aqueous solution. The color bars in the figures represent the visible region.

the simplest standard PCM scheme. One of the most employed models is the so called vertical excitation model (VEM) which is justified in the cases large-size compounds. Actually, the vibrational effects are important in determining both the position of the absorption maxima and the shape of the absorption structures. It has been shown that absorption bands in the spectra of simple organic compounds are typically redshifted between 0.1 and 0.2 eV in comparison to the vertical excitations.[85] Some recent studies investigated the origin of this red-shift, and found that the main reason can be ascribed to the frequency change between the ground and excited states in multidimensional systems, where vibrational frequencies in the excited states are systematically smaller than those of the ground states.[85] In all cases, in order to correctly consider this issue in our modeling, a numerical Hessian of the excited state in solution is needed, which is by no means practical for medium to large size molecules. It should be pointed out, however, that the vertical approximation is adopted in many previous studies dealing with relatively large-size molecular systems.[85]

Finally, for the excitations reported in Table 2 (gas phase column) we have also calculated the orbitals involved in the transitions in order to evaluate the possible charge transfer. The

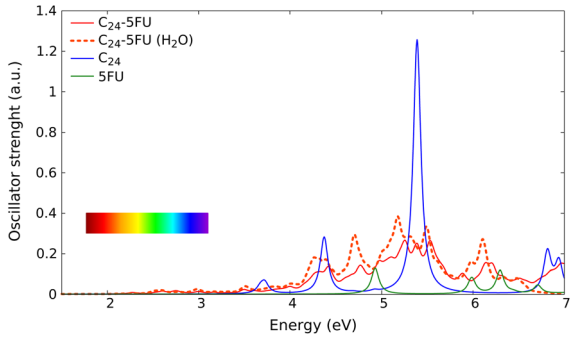


(a) Gas-phase absorption spectra of $C_{24}$-5FU (red line), $C_{24}$ (blue line) and 5FU (green line). The spectrum of $C_{24}$-5FU in aqueous solution is reported in dotted red line.

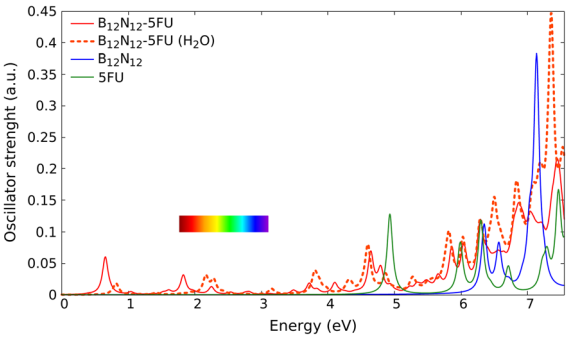


(b) Gas-phase absorption spectra of $B_{12}N_{12}$-5FU (red line), $B_{12}N_{12}$ (blue line) and 5FU (green line). The spectrum of $B_{12}N_{12}$-5FU in aqueous solution is reported in dotted red line.

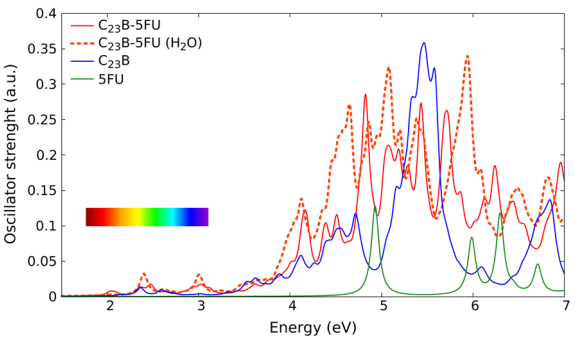


(c) Gas-phase absorption spectra of $C_{23}B$-5FU (red line), $C_{23}B$ (blue line) and 5FU (green line). The spectrum of $C_{23}B$-5FU in aqueous solution is reported in dotted red line.

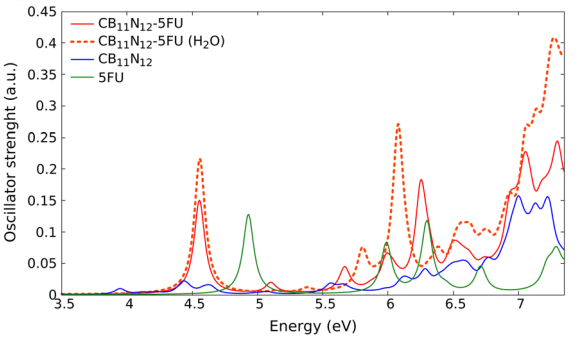


(d) Gas-phase absorption spectra of $CB_{11}N_{12}$-5FU (red line), $CB_{11}N_{12}$ (blue line) and 5FU (green line). The spectrum of $CB_{11}N_{12}$-5FU in aqueous solution is reported in dotted red line.

Fig. 5 Absorption spectra of the combined systems (a) $C_{24}$-5FU, (b) $B_{12}N_{12}$-5FU, (c) $C_{23}B$-5FU, (d) $CB_{11}N_{12}$-5FU after this work, compared to those of the free molecules (C/BN-carrier and 5FU). The spectra reported in solid line are calculated in gas phase while in dotted red line is shown the one of combined clusters in aqueous solution. The color bars in the (a–c) figures represent the visible region.

Table 1 Excitation energies ($E$, eV), wavelength ($\lambda$, nm) oscillator strength (O.S.), and molecular orbital contributions (with the corresponding weight in brackets) of selected transitions (onset and main peak), in gas and aqueous solution for free molecules

| Gas phase | | | | | Aqueous solution | | | | |
|---|---|---|---|---|---|---|---|---|---|
| Systems | $E$ (eV) | $\lambda$ (nm) | O.S. | MO contributions | Systems | $E$ (eV) | $\lambda$ (nm) | O.S. | MO contributions |
| T705 | 4.26 | 291.4 | 0.127 | H-1 → L (0.39) | T705 | 4.22 | 293.8 | 0.206 | H → L (0.48) |
| | 5.83 | 212.7 | 0.135 | H-1 → L + 1 (0.33) | | 5.74 | 215.8 | 0.163 | H → L + 1 (0.44) |
| | 7.94 | 156.2 | 0.248 | H-3 → L + 3 (0.12) | | 6.63 | 186.9 | 0.246 | H-5 → L (0.36) |
| | | | | H-2 → L + 5 (0.10) | | | | | |
| 5FU | 4.93 | 251.5 | 0.127 | H → L (0.46) | 5FU | 4.85 | 255.4 | 0.182 | H → L (0.47) |
| | 7.46 | 166.2 | 0.143 | H-1 → L + 4 (0.25) | | 7.37 | 168.3 | 0.345 | H-2 → L + 1 (0.29) |
| | | | | H-2 → LA + 1 (0.14) | | | | | |
| $C_{24}$ | 3.67 | 337.5 | 0.010 | H-1 → L + 3 (0.24) | $C_{24}$ | 3.66 | 338.8 | 0.017 | H → L + 3 (0.29) |
| | | | | H → L + 4 (0.19) | | | | | H-2 → L + 4 (0.23) |
| | | | | H-2 → L + 4 (0.16) | | | | | H-1 → L + 4 (0.19) |
| | 5.39 | 230.0 | 0.418 | H-10 → L (0.23) | | 5.31 | 233.7 | 0.531 | H-9 → L + 2 (0.31) |
| | | | | H-9 → L + 2 (0.15) | | | | | H-10 → L (0.16) |
| | | | | H-9 → L + 1 (0.14) | | | | | H-10 → L + 1 (0.15) |
| $B_{12}N_{12}$ | 6.35 | 195.3 | 0.035 | H-2 → L + 5 (0.19) | $B_{12}N_{12}$ | 6.39 | 194.0 | 0.052 | H-1 → L + 5 (0.21) |
| | | | | H-1 → L + 4 (0.16) | | | | | H-2 → L + 4 (0.18) |
| | 7.14 | 173.8 | 0.119 | H-6 → L + 2 (0.14) | | 7.16 | 173.1 | 0.155 | H-7 → L + 1 (0.14) |
| | | | | | | | | | H-8 → L + 2 (0.12) |
| $C_{23}B$ | 2.16 | 574.6 | 0.002 | HA-2 → LA + 2 (0.61) | $C_{23}B$ | 2.17 | 570.8 | 0.002 | HA-2 → LA + 2 (0.63) |
| | 5.47 | 226.5 | 0.144 | HA-10 → LA + 1 (0.19) | | 5.23 | 237.3 | 0.194 | HA-10 → LA + 2 (0.20) |
| | | | | HB-11 → LB + 2 (0.17) | | | | | HA-3 → LA + 3 (0.17) |
| | | | | HB-2 → LB + 7 (0.12) | | | | | HA-9 → LA (0.12) |
| $CB_{11}N_{12}$ | 3.95 | 314.1 | 0.009 | HA → LA + 2 (0.81) | $CB_{11}N_{12}$ | 4.01 | 309.0 | 0.012 | HA → LA + 2 (0.81) |
| | 7.00 | 177.1 | 0.045 | HB-1 → LB + 8 (0.21) | | 7.04 | 176.0 | 0.081 | HA-1 → LA + 8 (0.21) |
| | | | | HA-1 → LA + 7 (0.18) | | | | | HB → LB + 8 (0.21) |
| $Ga_{12}N_{12}$ | 2.31 | 537.7 | 0.001 | H → L (0.50) | $Ga_{12}N_{12}$ | 2.45 | 505.3 | 0.001 | H → L (0.5) |
| | 4.02 | 308.6 | 0.109 | H-14 → L (0.43) | | 4.08 | 304.0 | 0.188 | H-15 → L (0.45) |

orbitals for the onset transitions are reported in the final section of the ESI.†

### 3.1 C and BN clusters – T705 with adsorption

The first molecules that we analyze here are the ones first proposed in ref. 9, shown in Fig. 2a–d. As mentioned above, in this work we calculated the absorption spectra only of the molecules within TD-DFT. The calculations of the absorption spectra for all the molecules have been performed both in gas phase and in aqueous solution. The spectra obtained for those molecules are shown in Fig. 3. The comparison between the energies of the peaks calculated in this work (Gaussian16, B3LYP/6-31+G*) and the ones after ref. 9 (Gaussian09, B3LYP/6-31G**) are shown in Table 3.

In Fig. 3a is reported the absorption spectrum of the combined system in gas phase $C_{24}$-T705 (red line) and in aqueous solution $C_{24}$-T705 ($H_2O$) (red dotted line) in comparison with those of the free molecules in gas phase (the blue line is $C_{24}$ and the green line is T705). The energies of the peaks calculated for the combined system are shown in Table 2 and the ones for the free molecules are shown in Table 1. The first notable difference between combined molecule and free ones is the onset peak position, which is at 3.26 eV for the combined system in gas phase (3.22 eV in aqueous solution), 3.67 eV for $C_{24}$ in gas phase (3.66 eV in aqueous solution) and 4.26 eV for T705 in gas phase (4.22 eV in aqueous solution). We notice the presence of two peaks in the spectrum of the combined system positioned near the onset of the spectra for each free molecules. There are no notable differences in the energy of the main peak, that is near to the one of $C_{24}$. The main peak relative to the combined molecule results shifted passing from the gas phase to the aqueous solution (from 5.39 eV to 5.28 eV).

In Fig. 3b are reported the spectra of the combined system $B_{12}N_{12}$-T705 in gas phase and in aqueous solution $B_{12}N_{12}$-T705 ($H_2O$) and the spectra of the free molecules in gas phase only. At 2.69 eV in the spectrum of $B_{12}N_{12}$-T705 a small structure appears. In the proximity of the onset peak of T705 we still observe a peak in the spectrum of the combined molecule, shifted towards smaller energies (redshifted). We notice major overlaps towards larger energies.

In Fig. 3c are shown the spectra of the combined system $C_{23}B$-T705 in gas phase and in aqueous solution $C_{23}B$-T705 ($H_2O$) and the spectra of the free molecules in gas phase. The onset peak corresponding to $C_{23}B$-T705 is near the onset peak of

 

Table 2 Excitation energies ($E$, eV), wavelength ($\lambda$, nm) oscillator strength (O.S.), molecular orbital contributions (with the corresponding weight in brackets), character (CT/LE) of selected transitions (onset and main peak), in gas and aqueous solution for the combined systems

| Gas phase | | | | | Aqueous solution | | | | |
|---|---|---|---|---|---|---|---|---|---|
| Systems | $E$ (eV) | $\lambda$ (nm) | O.S. | MO contributions | Systems | $E$ (eV) | $\lambda$ (nm) | O.S. | MO contributions |
| $C_{24}$-T705 | 3.26 | 380.3 | 0.008 | H-3 → L + 1 (0.49) (CT) | $C_{24}$-T705 | 3.22 | 384.8 | 0.0003 | H → L + 3 (0.23)<br>H-1 → L + 3 (0.22) |
| | 5.39 | 229.9 | 0.333 | H-14 → L + 2 (0.13) (LE) | | 5.28 | 234.8 | 0.609 | H-14 → L (0.19) |
| $B_{12}N_{12}$-T705 | 2.69 | 461.3 | 0.009 | H → L (0.49) (CT) | $B_{12}N_{12}$-T705 | 3.59 | 345.1 | 0.006 | H → L (0.43) |
| | 4.10 | 302.5 | 0.196 | H-7 → L (0.42) (CT) | | 4.03 | 307.6 | 0.299 | H-3 → L (0.49) |
| $C_{23}B$-T705 | 2.15 | 577.0 | 0.002 | HB-1 → LB + 5 (0.24) (CT)<br>HA → LA + 4 (0.18) (CT) | $C_{23}B$-T705 | 2.09 | 593.0 | 0.001 | HB-1 → LB + 3 (0.20)<br>HA-1 → LA + 2 (0.16)<br>HA → LA + 3 (0.15) |
| | 4.10 | 302.1 | 0.139 | HA-10 → LA (0.26) (CT)<br>HB-9 → LB (0.24) (CT) | | 2.14 | 578.8 | 0.002 | HA → LA + 3 (0.32)<br>HB-1 → LB + 4 (0.32) |
| $CB_{11}N_{12}$-T705 | 2.32 | 534.9 | 0.049 | HA → LA + 9 (0.82) (LE) | $CB_{11}N_{12}$-T705 | 2.21 | 560.1 | 0.062 | HA → LA + 3 (0.88) |
| | 3.91 | 317.4 | 0.158 | HA-1 → LA (0.30) (CT)<br>HA → LA + 15 (0.28) (CT) | | 3.79 | 326.7 | 0.245 | HA → LA + 11 (0.52) |
| $Ga_{12}N_{12}$-5FU (ads) | 2.34 | 530.1 | 0.001 | H-1 → L (0.29) (CT)<br>H → L (0.16) (CT) | $Ga_{12}N_{12}$-5FU (ads) | 2.55 | 486.0 | 0.001 | H → L (0.48) |
| | 3.91 | 317.3 | 0.121 | H-13 → L + 1 (0.42) (LE) | | 4.03 | 307.4 | 0.177 | H-14 → L (0.40) |
| $Ga_{12}N_{12}$-5FU (cov) | 2.33 | 531.8 | 0.001 | H → L (0.49) (LE) | $Ga_{12}N_{12}$-5FU (cov) | 2.60 | 477.8 | 0.001 | H → L (0.49) |
| | 3.85 | 321.8 | 0.081 | H-12 → L (0.36) (LE) | | 4.29 | 289.3 | 0.119 | H-15 → L (0.34) |
| $C_{24}$-5FU | 2.27 | 546.2 | 0.006 | HB-2 → LB (0.45) (LE) | $C_{24}$-5FU | 2.28 | 542.9 | 0.002 | HB-3 → LB (0.34)<br>HA → LA + 2 (0.21) |
| | 5.25 | 236.2 | 0.103 | HA-2 → LA + 9 (0.15) (LE)<br>HA-1 → LA + 9 (0.08) (LE) | | 5.18 | 239.4 | 0.203 | HA → LA + 9 (0.12) |
| $B_{12}N_{12}$-5FU | 0.65 | 1894.0 | 0.059 | HB → LB (0.88) (CT) | $B_{12}N_{12}$-5FU | 0.82 | 1518.8 | 0.018 | HB-1 → LB (0.95) |
| | 6.29 | 197.0 | 0.060 | HB-11 → LB + 1 (0.36) (CT) | | 7.36 | 168.5 | 0.183 | HA-12 → LA + 1 (0.19)<br>HB-11 → LB + 2 (0.19) |
| $C_{23}B$-5FU | 2.03 | 610.9 | 0.005 | H → L + 2 (0.30) (LE)<br>H-2 → L + 1 (0.18) (LE) | $C_{23}B$-5FU | 2.40 | 517.3 | 0.029 | H-3 → L (0.48) |
| | 4.83 | 256.9 | 0.140 | H-1 → L + 8 (0.17) (LE)<br>H-11 → L + 2 (0.12) (LE) | | 4.65 | 266.4 | 0.182 | H-1 → L + 7 (0.39) |
| $CB_{11}N_{12}$-5FU | 4.56 | 272.2 | 0.149 | H → L (0.47) (LE) | $CB_{11}N_{12}$-5FU | 4.56 | 272.0 | 0.215 | H → L (0.48) |
| | 7.48 | 165.7 | 0.111 | H-14 → L (0.26) (LE)<br>H-4 → L + 10 (0.13) (CT) | | 6.08 | 204.0 | 0.241 | H → L + 6 (0.45) |

Table 3 Energies in eV of the peaks of the combined systems $C_{24}$-T705, $B_{12}N_{12}$-T705, $C_{23}B$-T705, $CB_{11}N_{12}$-T705 in comparison with those after ref. 9, in gas phase and in aqueous solution. In parenthesis the relative deviations have been reported

| Systems | $E^{gas}_{peak}$ (this work) | $E^{gas}_{peak}$ ref. 9 | $E^{H_2O}_{peak}$ (this work) | $E^{H_2O}_{peak}$ ref. 9 |
|---|---|---|---|---|
| $C_{24}$-T705 | 3.26 (+1.6%) | 3.21 | 3.22 (−0.9%) | 3.25 |
| $B_{12}N_{12}$-T705 | 4.10 (−0.9%) | 4.14 | 4.03 (−0.8%) | 4.06 |
| $C_{23}B$-T705 | 2.15 (−0.9%) | 2.17 | 2.09 (−5%) | 2.20 |
| $CB_{11}N_{12}$-T705 | 3.85 (+2%) | 3.76 | 3.90 (−4%) | 4.04 |

the free $C_{23}B$ (2.15 eV for the combined system and 2.16 eV for the free $C_{23}B$). We notice at 3.23 eV a peak in the $C_{23}B$-T705 that is not present in the other cases. We observe a redshift in the onset peak of the T705, more clear for $C_{23}B$-T705 ($H_2O$). At larger energies there are no notable differences.

In Fig. 3d are shown the spectra of the combined system $CB_{11}N_{12}$-T705 in gas phase and in aqueous solution $CB_{11}N_{12}$-T705 ($H_2O$) and the spectra of the free molecules in gas phase. In both phases, the spectrum of the combined molecule shows an onset peak at much smaller energies than the ones of the free

molecules. In the region where the onset peak of the free molecule is, we observe a peak in the combined system too. In the case of the combined molecule there is no evident difference between the spectrum for $CB_{11}N_{12}$-T705 and $CB_{11}N_{12}$-T705 ($H_2O$). In conclusion, in the analyzed configurations some peaks are present only for the combined systems and some notable differences take place between the absorption spectra of the free molecules and the ones of the combined molecules. Those differences can be used as an optical fingerprint to deduct if the molecules are truly combined. Furthermore, as shown in Table 3, the energies of the peaks for the combined molecule in gas phase here calculated are in fair agreement to those present in ref. 9. In fact we have a maximum deviation of 2% for the molecule in gas phase and of 5% for the molecule in aqueous solution.

### 3.2 GaN clusters-5FU

We analyze now the proposed molecules after ref. 6. Unlike the above analyzed molecules, in those clusters we have a carrier formed of gallium and nitrogen atoms. In the following we present the absorption spectra calculated in this work of two systems made of $Ga_{12}N_{12}$ combined with 5FU, the first *via* an adsorption (Fig. 2e) and the second *via* a covalent bond (Fig. 2f), both in gas phase and aqueous solution. In Table 4 has been reported the comparison between the energies of the peaks presented in ref. 6 (Gaussian09, BMK/6-31++G**) and the correspondent ones calculated in the present work (Gaussian16, B3LYP/6-31+G*).

In Fig. 4a we show the absorption spectrum of the adsorbed system $Ga_{12}N_{12}$-5FU. No large difference is present between the spectra of the combined molecule in gas phase and the free molecule $Ga_{12}N_{12}$. On the other hand, for the spectrum of combined molecule in aqueous solution $Ga_{12}N_{12}$-5FU ($H_2O$) we notice a blueshift of the main peak of the carrier and the presence of peaks at smaller energies that are not present for the $Ga_{12}N_{12}$. In the high energies region, the spectra of all the systems are similar.

In Fig. 4b we show the spectra of the covalent bonded system $Ga_{12}N_{12}$-5FU. As above, we notice small differences between the spectra of bonded molecule and free carrier in gas phase and we observe a blueshift of the peaks for the bonded molecule in aqueous solution. In the higher energies region we notice that the peaks present in the $Ga_{12}N_{12}$ spectrum are replaced by a single wide peak.

In conclusion, we find a good agreement in comparing the energies of the peaks calculated in the present work with the ones after ref. 6. The small differences in the data present in Table 4 can be ascribed to the different basis-set used for the calculations and to the different exchange–correlation functional used.

### 3.3 C and BN clusters – 5FU with covalent bond

Finally, we analyze the optical absorption spectra of the four original systems after this work (Fig. 5). We have obtained these systems (Fig. 2g–j) by forcing a covalent bond between the drug molecule (5FU) and the carrier (C/BN nanocluster). In Tables 1 and 2 we show some important details of the optical onset transitions and the main peaks of all the spectra of free and bound systems, in gas phase and aqueous solution.

In Fig. 5a we note that the spectrum of the combined system $C_{24}$-5FU is quite different from the ones of free $C_{24}$ and 5FU, for both energy position and height of the peaks. In particular, the absorption of $C_{24}$-5FU begins in the visible region at the energy of 2.27 eV, a value redshifted with respect to that of both the carrier (3.67 eV, NUV) and the drug (4.93 eV, MUV). The main feature of Fig. 5a is the strong reduction in height of the main peak of $C_{24}$ after its binding with 5FU. At this energy, 5.39 eV, we can find a peak of the combined system with a considerable smaller oscillator strength (from 0.418 to 0.064). Moreover, the nature of the transition is different because the involved molecular orbitals are not the same as for $C_{24}$. In particular, the transition for the combined system is between the orbitals HA-14 and LA, with a weight of 0.16, while those for $C_{24}$ are reported in Table 1. The main peak for $C_{24}$-5FU is located at 5.25 eV (in Table 2 more details about it). In this case the solvent effect in the spectrum of the combined system is not relevant. The onset and main peak for $C_{24}$-5FU ($H_2O$) are at similar energy than those in gas phase, with small differences in the O.S. and in the MO involved in the transitions (see Table 2). This fact can be of importance for applicative reasons: in fact the absence of the peak at 5.39 eV in the absorption spectrum can be interpreted as a clear optical fingerprint of the occurred molecular bond between $C_{24}$ and 5FU clusters.

In Fig. 5b we note that the absorption spectrum of $B_{12}N_{12}$-5FU is very different from that of the free $B_{12}N_{12}$ and 5FU systems. The combined system here analyzed is characterized by very different absorption structures, especially in the low energies region. In particular, the absorption of $B_{12}N_{12}$-5FU takes place in a range that cover the IR, the visible and the UV, while the absorption of free systems presents spectra mainly located in the UV region. In more detail, for the gas phase, the onset energy of the combined system is at 0.65 eV, very distant from the one of the drug (4.93 eV, MUV) and of the carrier (6.35 eV, FUV). For energies larger than 6 eV we can see similarities between the spectra. For example the main peak of $B_{12}N_{12}$-5FU in gas phase (6.29 eV) is at the same energy of a peak of the drug (6.29 eV, O.S. = 0.114, H → L + 2, weight = 0.44) and

Table 4 Energies in eV of the peaks of the combined systems in comparison with those after ref. 6 in aqueous solution. In parenthesis the relative deviations have been reported

| Systems | $E^{H_2O}_{peak,1}$ (this work) | $E^{H_2O}_{peak,1}$ ref. 6 | $E^{H_2O}_{peak,2}$ (this work) | $E^{H_2O}_{peak,2}$ ref. 6 |
|---|---|---|---|---|
| $Ga_{12}N_{12}$-5FU (ads) | 3.52 (+3%) | 3.43 | 4.73 (−0.4%) | 4.75 |
| $Ga_{12}N_{12}$-5FU (cov) | 3.54 (+2%) | 3.47 | 4.88 (+1.5%) | 4.81 |

it is near to the onset of the carrier (6.35 eV). Moreover, the combined system presents a major peak at 7.44 eV¶ near to the main peaks of the free systems $B_{12}N_{12}$ (7.14 eV) and 5FU (7.46 eV). We see from Table 2 that the nature of these transitions is different. On the other hand, the solvent effect in the TD-DFT calculations leads to some differences in the onset and in the main peak of the combined system with respect to the gas phase. The onset peak is blueshifted (from 0.65 eV to 0.82 eV) and its oscillator strength is reduced (from 0.059 to 0.018); the main peak is at higher energies (from 6.29 eV to 7.36 eV) near to the before mentioned peak at 7.44 eV. Also in this case, the presence of structures in a more than 4 eV extended region below the absorption edge of 5FU is a clear optical fingerprint of the occurred molecular bond between $B_{12}N_{12}$ and 5FU.

In Fig. 5c we note that, for the combined system $C_{23}$B-5FU, the initial part of the spectrum is similar to that of the carrier $C_{23}$B. This behavior occurs up to 4.5 eV, for an energy range in which the free biomolecule is not absorbing. The onset energy for both the combined system and the carrier is in the visible region, respectively at 2.03 eV and 2.16 eV. The spectrum of $C_{23}$B-5FU at energies larger than 4.5 eV differs slightly from the spectra of free molecules. In particular, it presents some new absorption structures. The main peak of $C_{23}$B-5FU (4.83 eV) is only 0.1 eV redshifted with respect to the energy of the onset for the drug (4.93 eV). Moreover, near the carrier MP energy position (5.47 eV), there is a peak of the combined system ($E = 5.42$ eV, O.S. $= 0.097$, H-11 $\rightarrow$ L + 3, weight $= 0.33$). The spectrum of $C_{23}$B-5FU ($H_2O$) presents peaks at energies slightly different from those for the gas phase. In more detail, the onset peak is blueshifted (from 2.03 eV to 2.40 eV) while the main peak results redshifted (from 4.83 eV to 4.65 eV). In this case no clear and distinguishable optical difference could be found for the considered clusters either in gas phase and in aqueous solution.

In Fig. 5d we see that the $CB_{11}N_{12}$-5FU begins its absorption in the MUV at 4.56 eV. This is the only case, with respect to the here studied clusters, in which the onset energy lies in the UV region at a value placed in the middle between the peaks of free molecules. In the three previous cases instead, the onset for the combined system was always at lower energy than for the free molecules and it lied in the visible or IR region. Here, otherwise, the onset of $CB_{11}N_{12}$-5FU is blueshifted of +15% and redshifted of −7% as compared, respectively, to those of the cluster (3.95 eV, NUV) and the drug (4.93 eV, MUV). In the regions around 6 eV and 7 eV we find also some overlaps of peaks of the free and bound systems. In this case the solvent effect is more significant in the region beyond 5.5 eV. The onset results at the same energy (4.56 eV) as that found for the gas phase. However, the oscillator strength is almost double (from 0.149 to 0.215). Beyond 5.5 eV, for $CB_{11}N_{12}$-5FU ($H_2O$) we observe a shift of the peaks (for example that around 6.25 eV) and to an average increase of the oscillator strengths. In this particular case the presence of the peak at 4.56 eV can be considered as the optical evidence of the realised drug/carrier bond.

¶ Around this energy there are several roots that determined a broad Lorentzian structure. The root with larger oscillator strength is characterized by: $E = 7.44$ eV, O.S. $= 0.032$, HA-5 $\rightarrow$ LA + 6, weight $= 0.08$.

### 3.4 Long-range corrected optical properties

We have performed some test calculations for 5FU systems using the long-range corrected CAM-B3LYP exchange–correlation functional.

As we show in Fig. 6, the corresponding spectra presents basically just an almost rigid shift of the order of ∼0.1 to ∼0.4 eV and some small amplitude variations in the absorption features. The shift appears of the same order of those found in ref. 86 using CAM-B3LYP.

For the scope and the level of this work the differences between the two calculations are small enough to guarantee the low energy same pattern. For this reason we can still consider valid our previous B3LYP results.

## 4. Additional computational details, tests, and open issues

To give a more general (and chemical) insight in the results of the present paper, the MOs for the onset transitions relative to a large subset of the studied systems, along with a description of the CT transitions, have been reported in the ESI.† Moreover, the details of the transitions have been extensively reported in Tables 1 and 2. Take in consideration that we also made the comparison of our results with those after ref. 6 and 9. We have

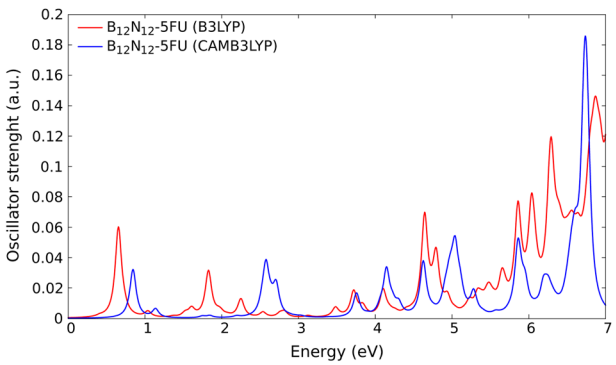


(a) Gas-phase absorption spectra of $B_{12}N_{12}$-5FU calculated with B3LYP (red line) and CAM-B3LYP (blue line).

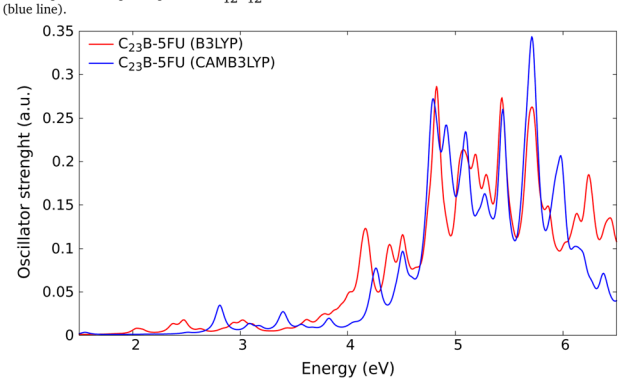


(b) Gas-phase absorption spectra of $C_{23}$B-5FU calculated with B3LYP (red line) and CAM-B3LYP (blue line).

Fig. 6 Absorption spectra calculated with different exchange–correlation functional; comparison for (a) $B_{12}N_{12}$-5FU and (b) $C_{23}$B-5FU.

found a good agreement with the calculations of those references, proving that our method is valid and can be used for studying similar drug delivery systems, as the ones original from our work. In addition, we calculated some properties that are not present in the literature that can be used to provide other information on the systems of interest, *e.g.*, full spectra representation and some additional peaks information.

We performed also different additional convergence tests: the average number of states included in the calculations are 350 for each system, using the Casida formalism to calculate the absorption spectra.

In the cases of CT character, the theory here adopted presents some limitations (as reported, *e.g.*, in ref. 84) and for this reason some CT states may be affected by an unfair description. Moreover, the number of states calculated may be not sufficient to completely characterize the high energy region of the absorption spectra of some molecules. On the other hand, it is out of the scope of this work a in depth study of the high energy or Rydberg transitions.

To validate further our method, we have performed additional calculations with a larger basis set for the wave-function representation in some configurations and the resulting spectra are almost identical to the ones we reported in this article produced with the smaller basis set.

Considering the possible discrepancies arising for some CT transitions after the use of the TDDFT-B3LYP scheme, we performed additional TDDFT CAM-B3LYP spectra calculation (Section 3.4). The comparison with the TDDFT-B3LYP spectrum demonstrates that the CAM-B3LYP absorption spectrum present the same structure and main peaks with a small blue-shift. We reached these conclusions after comparing tha absorption spectra for some systems, *e.g.*, the $B_{12}N_{12}$-5FU and the $C_{23}$B-5FU systems, (reported respectively in Fig. 6a and b).

All the spectra have been obtained by the convolution of Lorentzian curves (FHWM of 0.05 eV) with the single eigenvalues' peaks obtained by the output of Gaussian16. The broadening value is obtained by a trade-off between the plots readability and the need to ensure that most of the peaks are resolved.

Moreover, we decided to add in the ESI† the coordinates for some important cases in order to guarantee the reproducibility of the results. Hereby we confirm that the here proposed method permits to know for the first time, for several different molecular systems of importance for the drug delivery, how their electronic and optical properties change following the establishment of a bond between the carrier and the drug molecule. Moreover, the possibility to compare to previous works for some systems confirmed the validity of the methodology we applied.

Finally, in some of the studied systems there is the occurrence of possible multireference character (MC) states. However, since this phenomenon occurs only in a very limited number of the molecules under study, this fact does not affect dramatically the general conclusions of the paper. We have already planned a new computational campaign in which we will address in a deeper way this particular issue using more refined computational schemes.

# 5. Conclusions

We propose in the present work a computational study of the optical absorption of nanostructured clusters of interest for drug delivery applications. We considered a group of combined drug/carrier clusters which have been demonstrated stable after previous computational studies. The remaining systems show stable geometries after the present study. We, in some cases, observed the appearance of new peaks in the spectra of the combined systems or red or blue shift effects in the already existing structures. The changes in the absorption spectra could play the role of an optical signature helping to verify the correct occurred bonding needed for drug delivery and for tracking the combined clusters once formed in solution. Possible future developments of the present work could be the study of the release mechanisms of the drug at the target, the application of more refined models for the water solvent, the extension of the same analysis to different solvents.

# Conflicts of interest

There are no conflicts to declare.

# Acknowledgements

G. C. acknowledges collaboration with "Progetti biennali d'Ateneo UniCa finanziati dalla Fondazione di Sardegna annualità 2020: molecular simulations and machine learning in bio- and medical physics". G. C., A. A. P., F. S. acknowledge partial financial support from the IDEA-AISBL-Bruxelles. The authors acknowledge ISCRA-CINECA facility within the ISCRA-C 2021 projects HP10CDZJIB/HP10CS0OT2/HP10C8WASP. F. S. acknowledges that this article was produced while attending the PhD programme in Physics at the University of Cagliari, Cycle XXXVIII, with the support of a scholarship financed by the Ministerial Decree no. 351 of 9th April 2022, based on the NRRP – funded by the European Union – NextGenerationEU – Mission 4 "Education and Research", Component 1 "Enhancement of the offer of educational services: from nurseries to universities" – Investment 4.1 "Extension of the number of research doctorates and innovative doctorates for public administration and cultural heritage".

# Notes and references

1 P. Wang, G. Yan, X. Zhu, Y. Du, D. Chen and J. Zhang, *Nanomaterials*, 2021, **11**, 115.
2 B. T. Tomić, C. S. Abraham, S. Pelemiš, S. J. Armaković and S. Armaković, *Phys. Chem. Chem. Phys.*, 2019, **21**, 23329–23337.
3 M. Moradi, A. A. Peyghan, Z. Bagheri and M. Kamfiroozi, *J. Mol. Model.*, 2012, **18**, 3535–3540.
4 T. Dinadayalane and J. Leszczynski, in *Fundamental Structural, Electronic, and Chemical Properties of Carbon Nanostructures: Graphene, Fullerenes, Carbon Nanotubes, and Their Derivatives*, Springer, 2012, pp. 793–867.

5 D. S. Sabirov, A. D. Zakirova, A. A. Tukhbatullina, I. M. Gubaydullin and R. G. Bulgakov, *RSC Adv.*, 2013, **3**, 1818–1824.
6 N. Wazzan, K. Soliman and W. Abdel Halim, *J. Mol. Model.*, 2019, **25**, 265.
7 A. Zerenturk and S. Berber, *Europhys. Lett.*, 2013, **103**, 16003.
8 Y. Arakawa and S. Kako, *Phys. Status Solidi A*, 2006, **203**, 3512–3522.
9 K. A. Soliman and S. A. Aal, *Diamond Relat. Mater.*, 2021, **117**, 108458.
10 Y. Furuta, K. Takahashi, K. Shiraki, K. Sakamoto, D. F. Smee, D. L. Barnard, B. B. Gowen, J. G. Julander and J. D. Morrey, *Antiviral Res.*, 2009, **82**, 95–102.
11 Y. Furuta, B. B. Gowen, K. Takahashi, K. Shiraki, D. F. Smee and D. L. Barnard, *Antiviral Res.*, 2013, **100**, 446–454.
12 S. J. Smither, L. S. Eastaugh, J. A. Steward, M. Nelson, R. P. Lenk and M. S. Lever, *Antiviral Res.*, 2014, **104**, 153–155.
13 Y.-X. Du and X.-P. Chen, *Clin. Pharmacol. Ther.*, 2020, **108**, 242–247.
14 Y. Furuta, B. B. Gowen, K. Takahashi, K. Shiraki, D. F. Smee and D. L. Barnard, *Antiviral Res.*, 2013, **100**, 446–454.
15 M. Milczarek, K. Wiktorska, L. Mielczarek, M. Koronkiewicz, A. Dąbrowska and K. Lubelska, *Food Chem. Toxicol.*, 2018, **111**, 1–8.
16 H. Uetsuka, M. Haisa, M. Kimura, M. Gunduz, Y. Kaneda, T. Ohkawa, M. Takaoka, T. Murata, T. Nobuhisa, T. Yamatsuji, J. Matsuoka, N. Tanaka and Y. Naomoto, *Exp. Cell Res.*, 2003, **289**, 27–35.
17 L. Metterle, C. Nelson and N. Patel, *J. Am. Acad. Dermatol.*, 2016, **74**, 552–557.
18 Sauraj, V. Kumar, B. Kumar, F. Deeba, S. Bano, A. Kulshreshtha, P. Gopinath and Y. S. Negi, *Int. J. Biol. Macromol.*, 2019, **128**, 204–213.
19 H. W. Kroto, J. R. Heath, S. C. O'Brien, R. F. Curl and R. E. Smalley, *Nature*, 1985, **318**, 162–163.
20 H. W. Kroto, *Angew. Chem., Int. Ed. Engl.*, 1997, **36**, 1578–1593.
21 H. W. Kroto, *Nature*, 1987, **329**, 529–531.
22 A. Popov, in *Structures and Stability of Fullerenes, Metallofullerenes, and Their Derivatives*, Springer, 2017, pp. 1031–1096.
23 Y. Chang, J. Zhang, H. Sun, B. Hong, Z. An and R. Wang, *Int. J. Quantum Chem.*, 2005, **105**, 142–147.
24 E. A. Rohlfing, D. M. Cox and A. Kaldor, *J. Chem. Phys.*, 1994, **81**, 3322–3330.
25 F. Diederich, R. Ettl, Y. Rubin, R. L. Whetten, R. Beck, M. Alvare, S. Anz, D. Sensharma, F. Wudl, K. C. Khemani and A. Koch, *Science*, 1991, **252**, 548–551.
26 K. Kikuchi, N. Nakahara, T. Wakabayashi, M. Honda, H. Matsumiya, T. Moriwaki, S. Suzuki, H. Shiromaru, K. Saito, K. Yamauchi, I. Ikemoto and Y. Achiba, *Chem. Phys. Lett.*, 1992, **188**, 177–180.
27 T. Kimura, T. Sugai, H. Shinohara, T. Goto, K. Tohji and I. Matsuoka, *Chem. Phys. Lett.*, 1995, **246**, 571–576.
28 Y. Miyake, T. Minami, K. Kikuchi, M. Kainosho and Y. Achiba, *Mol. Cryst. Liq. Cryst.*, 2000, **340**, 553–558.
29 R. Taylor, G. J. Langley, A. G. Avent, T. J. S. Dennis, H. W. Kroto and D. R. M. Walton, *J. Chem. Soc.*, 1993, **2**, 1029–1036.
30 F. Jensen and H. Toflund, *Chem. Phys. Lett.*, 1993, **201**, 89–96.
31 T. Oku, M. Kuno, H. Kitahara and I. Narita, *Int. J. Inorg. Mater.*, 2001, **3**, 597–612.
32 V. Mahamiya, A. Shukla and B. Chakraborty, *J. Alloys Compd.*, 2022, **897**, 162797.
33 S. Kaviani, S. Shahab, M. Sheikhi, V. Potkin and H. Zhou, *Comput. Theor. Chem.*, 2021, **1201**, 113246.
34 G. Seifert, P. Fowler, D. Mitchell, D. Porezag and T. Frauenheim, *Chem. Phys. Lett.*, 1997, **268**, 352–358.
35 T. Oku, A. Nishiwaki, I. Narita and M. Gonda, *Chem. Phys. Lett.*, 2003, **380**, 620–623.
36 O. Stéphan, Y. Bando, A. Loiseau, F. Willaime, N. Shramchenko, T. Tamiya and T. Sato, *Appl. Phys. A: Mater. Sci. Process.*, 1998, **67**, 107–111.
37 D. Golberg, Y. Bando, O. Stéphan and K. Kurashima, *Appl. Phys. Lett.*, 1998, **73**, 2441–2443.
38 M. Javan, A. Soltani, Z. Azmoodeh, N. Abdolahi and N. Gholami, *RSC Adv.*, 2016, **6**, 104513–104521.
39 E. Tazikeh, A. Soltani, M. T. Baei, M. Javan and S. Moazen Rad, *Adsorption*, 2018, **24**, 585–593.
40 E. Vessally, S. A. Siadati, A. Hosseinian and L. Edjlali, *Talanta*, 2017, **162**, 505–510.
41 A. Soltani, M. T. Baei, E. Tazikeh and A. Pahlevani, *Superlattices Microstruct.*, 2014, **75**, 716–724.
42 M. R. Mohammadi, A. Nojoomi, M. Mozafari, A. Dubnika, M. Inayathullah and J. Rajadas, *J. Mater. Chem. B*, 2017, **5**, 3995–4018.
43 A. Hosseinian, E. Vessally, S. Yahyaei, L. Edjlali and A. Bekhradnia, *J. Cluster Sci.*, 2017, **28**, 2681–2692.
44 L. Wang, Z. Wang, L. Cao and K. Ge, *Biosaf. Health*, 2022, **4**, 161–170.
45 R. Delshadi, A. Bahrami, D. J. McClements, M. D. Moore and L. Williams, *J. Controlled Release*, 2021, **331**, 30–44.
46 R. Bolskar, in *Fullerenes for Drug Delivery*, Springer, 2016, pp. 1267–1281.
47 H. Kazemzadeh and M. Mozafari, *Drug Discovery Today*, 2019, **24**, 898–905.
48 E. Giusto, L. Žárská, D. F. Beirne, A. Rossi, G. Bassi, A. Ruffini, M. Montesi, D. Montagner, V. Ranc and S. Panseri, *Nanomaterials*, 2022, **12**, 2372.
49 H. Wang, P. Agarwal, S. Zhao, J. Yu, X. Lu and X. He, *Nat. Commun.*, 2015, **6**, 10081.
50 J. Shi, H. Zhang, L. Wang, L. Li, H. Wang, Z. Wang, Z. Li, C. Chen, L. Hou, C. Zhang and Z. Zhang, *Biomaterials*, 2013, **34**, 251–261.
51 A. Soltani, A. Sousaraei, H. Balakheyli, M. Eskandari and M. Javan, *New J. Chem.*, 2016, **40**, 7018–7026.
52 M. Alpater, Z. Al-Sawaff and F. Kandemirli, *Global J. Eng. Technol. Adv.*, 2021, **9**, 77–85.
53 W. Kohn, *Rev. Mod. Phys.*, 1999, **71**, S59–S77.
54 R. O. Jones and O. Gunnarsson, *Rev. Mod. Phys.*, 1989, **61**, 689–746.

55 M. E. Casida, in *Time-Dependent Density Functional Response Theory for Molecules*, World Scientific Publishing, 1995, vol. 1, ch. 5, pp. 155–192.
56 G. Onida, L. Reining and A. Rubio, *Rev. Mod. Phys.*, 2002, **74**, 601–659.
57 M. Palummo, C. Hogan, F. Sottile, P. Bagalá and A. Rubio, *J. Chem. Phys.*, 2009, **131**, 084102.
58 M. Frisch, et al., *Gaussian16*, 2016.
59 R. Ditchfield, W. J. Hehre and J. A. Pople, *J. Chem. Phys.*, 1971, **54**, 724–728.
60 A. D. Becke, *J. Chem. Phys.*, 1993, **98**, 5648.
61 C. Lee, W. Yang and R. G. Parr, *Phys. Rev. B: Condens. Matter Mater. Phys.*, 1988, **37**, 785–789.
62 R. Cardia, G. Malloci, A. Mattoni and G. Cappellini, *J. Phys. Chem. A*, 2014, **118**, 5170–5177.
63 N. Dardenne, R. Cardia, J. Li, G. Malloci, G. Cappellini, X. Blase, J.-C. Charlier and G.-M. Rignanese, *J. Phys. Chem. C*, 2017, **121**, 24480–24488.
64 P. Mocci, R. Cardia and G. Cappellini, *Phys. Chem. Chem. Phys.*, 2019, **21**, 16302–16309.
65 G. Cappellini, A. Bosin, G. Serra, J. Furthmüller, F. Bechstedt and S. Botti, *ACS Omega*, 2020, **5**, 13268–13277.
66 A. Kumar, R. Cardia and G. Cappellini, *Cellulose*, 2017, **25**, 2191–2203.
67 L. Stagi, D. Chiriu, M. Scholz, C. M. Carbonaro, R. Corpino, A. Porcheddu, S. Rajamaki, G. Cappellini, R. Cardia and P. C. Ricci, *Spectrochim. Acta, Part A*, 2017, **183**, 348–355.
68 R. Cardia, G. Malloci, G.-M. Rignanese, X. Blase, E. Molteni and G. Cappellini, *Phys. Rev. B: Condens. Matter Mater. Phys.*, 2016, **93**, 235132.
69 R. Cardia, G. Cappellini, M. Valentini and E. Pieroni, *Phys. Chem. Chem. Phys.*, 2022, **24**, 25547–25554.
70 R. Cardia, G. Malloci, A. Bosin, G. Serra and G. Cappellini, *Chem. Phys.*, 2016, **478**, 8–13.
71 E. Pinna, C. Melis, A. Antidormi, R. Cardia, E. Sechi, G. Cappellini, M. d'Ischia, L. Colombo and G. Mula, *Int. J. Mol. Sci.*, 2017, **18**, 1567.
72 A. Antidormi, G. Aprile, G. Cappellini, E. Cara, R. Cardia, L. Colombo, R. Farris, M. d'Ischia, M. Mehrabanian, C. Melis, G. Mula, A. Pezzella, E. Pinna and E. Redolfi Riva, *J. Phys. Chem. C*, 2018, **122**, 28405–28415.
73 A. Kumar, G. Cappellini and F. Delogu, *Cellulose*, 2019, **26**, 1489–1501.
74 P. Mocci, R. Cardia and G. Cappellini, *J. Phys.: Conf. Ser.*, 2019, **1226**, 012016.
75 P. Mocci, R. Cardia, A. Bosin and G. Cappellini, *J. Phys.: Conf. Ser.*, 2020, **1548**, 012028.
76 P. Mocci, R. Cardia and G. Cappellini, *New J. Phys.*, 2018, **20**, 113008.
77 P. Mocci, R. Cardia and G. Cappellini, *J. Phys.: Conf. Ser.*, 2018, **956**, 012020.
78 B. X. Vuong, N. Hajali, A. Asadi, A. A. Baqer, S. K. Hachim and G. Canli, *Inorg. Chem. Commun.*, 2022, **141**, 109558.
79 J. Tomasi, B. Mennucci and R. Cammi, *Chem. Rev.*, 2005, **105**, 2999–3094.
80 E. Molteni, G. Cappellini, G. Onida and G. Fratesi, *Phys. Rev. B*, 2017, **95**, 075437.
81 E. Molteni, G. Fratesi, G. Cappellini and G. Onida, *Phys. Status Solidi B*, 2017, **255**, 1700497.
82 K. Seino, W. G. Schmidt, M. Preuss and F. Bechstedt, *J. Phys. Chem. B*, 2003, **107**, 5031–5035.
83 K. Seino, W. G. Schmidt and F. Bechstedt, *Phys. Rev. B: Condens. Matter Mater. Phys.*, 2004, **69**, 245309.
84 S. Kümmel, *Adv. Energy Mater.*, 2017, **7**, 1700440.
85 Q. Alkhatib, W. Helal and A. T. Afaneh, *New J. Chem.*, 2022, **46**, 7682–7694.
86 T. Yanai, D. P. Tew and N. C. Handy, *Chem. Phys. Lett.*, 2004, **393**, 51–57.